TWO-DIMENSIONAL NUMERICAL STUDY ON COMBUSTION CHARACTERISTICS OF NH_3/H_2/AIR COMBUSTION IN A TWO-LAYER POROUS BURNER

Peng DONG[a], Xiaohang QU [*a], Xing LI [*b], Junrui SHI[a], Jun LI[b], Danan CHEN[b], Chengdong HE[b]

[a] School of Transportation and Vehicle Engineering, Shandong University of Technology, Zibo 255049, China

[b] Guangzhou Institute of Energy Conversion, Chinese Academy of Sciences, Guangzhou 510640, China

[*]Corresponding authors; E-mail: quxiaohang@outlook.com (XH.Q.); lixing@ms.giec.ac.cn (X.L.)

This study primarily investigates the NH_3/H_2/air combustion characteristics within a two-layer porous burner employing a two-dimensional model with a detailed kinetics. The effects of inlet velocity ($u_{g,in}$) and blending ratio on the combustion characteristics are systematically examined. It is shown that the gas temperature continuously increases from the inlet before entering the reaction zone due to the heat recirculation via porous medium, thereby expanding the stable combustion limit and lean flammability limit of the mixture. Under a hydrogen blending ratio of 20%, the NH_3/H_2 achieves stable combustion in the burner for $u_{g,in}$=0.2 m/s-0.8 m/s and the equivalence ratio range of 0.5-0.65. The stable flames are stabilized just behind the interface when $u_{g,in}$<0.9 m/s, then the flames are stabilized towards the burner outlet. The emission of NO increases monotonically with $u_{g,in}$, ranging from approximately 5320 ppm at $u_{g,in}$=0.2 m/s to over 18700 ppm at $u_{g,in}$=0.8 m/s. In contrast, the NO_2 emissions remain relatively stable across the range of inlet velocities studied, fluctuating around 100 ppm. The flame tends to be stabilized towards the upstream as the equivalence ratio is increasing from 0.55 to 0.65 under $u_{g,in}$=0.8 m/s and blending ratio of 0.2, while the NO is increasing linearly from 14310 ppm to 19690 ppm with the equivalence ratio. A preliminary experimental validation is conducted and the same variation trend with the experiment is obtained, but the deviation between the two methods is obvious. This study contributes to enhancing combustion stability, extending flammability limits, and reducing nitrogen oxide emissions, providing key theoretical support for the development of efficient, low-carbon combustion technologies.

Key words: *NH_3/H_2 combustion; Porous media; Heat recirculating; Combustion characteristic*

1. Introduction

The use of traditional fossil fuels has led to severe environmental impacts and climate change. Among these, carbon dioxide emissions have led to a rise in global temperatures. In order to build a zero-carbon emission energy and industrial system, it is becoming a new trend to reduce carbon

emissions. Among various alternative fuels, NH_3, as a carbon free fuel, produces N_2 and H_2O as complete combustion products. Therefore, the use of NH_3 is beneficial for reducing carbon emissions [1]. NH_3 has the advantages of high energy volume density, significant energy storage effect, large production volume, and easy liquefaction and storage transportation, which has gradually attracted extensive research [2].

However, NH_3 combustion also has its own limitations, such as difficulty in ignition and poor combustion stability under conventional conditions, and the risk of high NOx emissions during NH_3 combustion [3]. To solve the problems in ammonia combustion, improve combustion stability and expand stable combustion limits, many researchers have proposed various new combustion technologies for NH_3 utilizations [4-9].

Porous media combustion technology, as an efficient combustion technology, has the advantages of heat accumulation and heat recirculating [10-13]. This is due to the fact that porous media have a large internal surface area, which can enhance the heat transfer between gas-solid phase, and their internal structure can also enhance gas diffusion and heat transfer. Therefore, the flame temperature will be significantly increased compared to free space, achieving super adiabatic combustion [10].

Nozari et al [14] studied the premixed combustion of NH_3/H_2 in porous media under standard temperature and pressure conditions. The results showed that under an equivalence ratio of 0.9-1.5 and ammonia concentrations of 60%-90%, the burner could achieve stable combustion of ammonia fuel.

Lv et al. [15] numerically studied the effect of reactants heating on the lean flammability limit (LEL) of pure NH_3 combustion in a two-layer porous burner. The results demonstrated that the preheating temperature exerts a significant influence on the expansion of the LEL, which was successfully broadened from an equivalence ratio of 0.54 to 0.08 as the preheating temperature is increased from 400 K to 1000 K.

Rocha et al. [16] experimentally investigated the combustion characteristics of ammonia blended with methane and hydrogen in a two-layer burner. They found that, in the case of hydrogen-blended combustion, the NOx emissions reached their maximum values when the volumetric fraction of hydrogen was 0.2 and 0.5. They compared the predictive performance of three chemical kinetic mechanisms [17-19] for NOx formation and observed that, although the predicted trends were consistent with the experimental data, the NOx predictions from all three models were significantly higher than the measured values. They attributed this discrepancy to limitations in both the chemical kinetic models and their self-developed one-dimensional mathematical model.

Vignat et al. [20] experimentally investigated the effects of hydrogen blending ratio on the LFL and pollutant emissions of ammonia combustion in a porous burner. They found that as the hydrogen blending ratio increased from 0.1 to 0.4, the LFL was progressively extended. When the hydrogen blending ratio reached 0.4 or 0.3, the overall equivalence ratio could be expanded to a range of approximately 0.5-0.55. Furthermore, it was observed that NOx emissions exhibited a decreasing trend under conditions where the flame approached blowout or when the inlet mass flow rate was increased.

Subsequently, Vignat et al. [21] investigated the combustion characteristics of ammonia and ammonia blends in a two-layer porous medium by extending the length of the porous medium and insulating the burner. They found that the modified burner enabled stable combustion of pure ammonia. The NOx emissions exhibited a parabolic distribution with respect to the equivalence ratio, whereas the trend of escaped ammonia was inversely related to that of NOx.

Chen et al. [22] investigated the combustion characteristics of ammonia blended with hydrogen

over an equivalence ratio range of 0.9-1.2 using a two-dimensional model based on the volume-averaged method for ammonia/hydrogen combustion. They found that the properties of the porous medium had a significant impact on the combustion process. Specifically, as the thermal conductivity of the porous medium increased, the peak temperature decreased and the flame shifted upstream. Moreover, with an increasing hydrogen blending ratio, the peak temperature increased, leading to higher NOx emissions. Recently, Jiang et al. [23, 24] experimentally studied the flame stability at the surface of the burner outlet, it was found that changes in the equivalence ratio resulted in distinct flame states

Although extensive research has been conducted on ammonia combustion in porous media, these studies have mainly focused on demonstrating the role of porous media in stabilizing the combustion of ammonia fuel with a high equivalence ratio, a systematic numerical investigation on the combustion characteristics of ammonia in porous media remains necessary. The purpose of this study is to investigate the combustion characteristics of ammonia and hydrogen mixtures under different flow rates and equivalence ratios using numerical simulation methods - including temperature distribution, flame structure, and other related parameters - which requires more in-depth research. The study of ammonia-hydrogen blended combustion in porous media contributes to enhancing combustion stability, extending flammability limits, and reducing nitrogen oxide emissions, providing key theoretical support for the development of efficient, low-carbon combustion technologies.

2 Numerical simulations

2.1 Physical model

In order to investigate the combustion characteristics of NH_3/H_2/air in porous burner and analyze the influence of factors such as inlet velocity and equivalence ratio on porous media combustion, numerical simulation is conducted on a two-layer porous burner based on the Volume Averaged Method (VAM) with a detailed kinetics. As shown in Fig. 1, the porous burner is a cylindrical shape with an inner diameter of 60 mm and a total length of 80 mm. The porous material at the downstream of the burner is 40 PPI SIC foam with thickness of 40 mm, serving as preheating zone, whereas the upstream of the burner is 20 PPI SIC foam with the same thickness. The physical property parameters of the SIC used in this study are shown in Tab. 1.

Tab. 1. Physical property parameters of porous media [20, 21]

Material	SiC	SiC
Pore Density [PPI]	40	20
Thickness [mm]	40	40
Porosity ε [%]	84.1	85.3
Average pore size d_p [mm]	0.5	1.3
Density ρ_s [kgm^{-3}]	2620	2620
Emissivity coefficient	0.85	0.85
Effective thermal conductivity [Wm-1K-1]	2.8	3.3

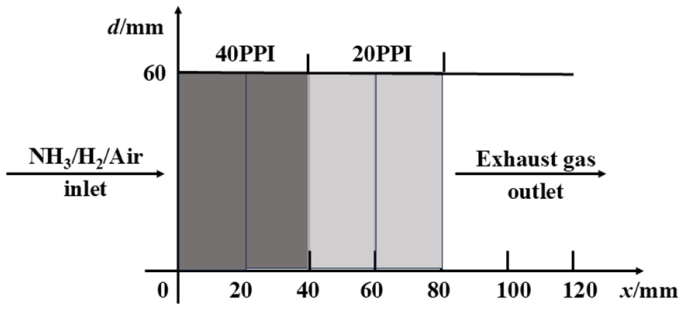

Fig. 1 Schematic diagram of a double-layer porous media burner

2.2 Mathematical model

To reduce the computational burden, the simulations are based on an axisymmetric two-dimensional model. To simplify the problem, some assumptions are introduced as follows,

(1) Porous media are isotropic, inert, and homogeneous optical thick media;

(2) The dispersion effect of mixture is ignored;

(3) The mixture is an incompressible ideal gas, the gas radiation is not considered;

(4) The gas flow in porous media is laminar;

(5) The solid radiation is computing based on the Rosseland model.

Under the stated assumptions, the following set of governing equations is obtained [10]:

Ideal gas equation of state

$$\rho_{\mathrm{g}} = \frac{P}{\mathrm{R}T_g} \tag{1}$$

where ρ_{g}, T_{g} are gas density and temperature, respectively. The P denotes pressure.

Continuity equation

$$\frac{\partial\left(\varepsilon\rho_{\mathrm{g}}u_{\mathrm{g}}\right)}{\partial x}+\frac{1}{r}\frac{\partial\left(\varepsilon\rho_{\mathrm{g}}rv_{\mathrm{g}}\right)}{\partial r}=0 \tag{2}$$

where ε is the porosity, u_{g} and v_{g} are the axial and radial velocity, respectively.

Axial momentum

$$\frac{\partial\left(\varepsilon\rho_{\mathrm{g}}u_{\mathrm{g}}u_{\mathrm{g}}\right)}{\partial x}+\frac{1}{r}\frac{\partial\left(\varepsilon\rho_{\mathrm{g}}ru_{\mathrm{g}}v_{\mathrm{g}}\right)}{\partial r}=-\varepsilon\frac{\partial P}{\partial x}+\frac{\partial}{\partial x}\left(\mu\frac{\partial u_{\mathrm{g}}}{\partial x}\right)+\frac{1}{r}\frac{\partial}{\partial r}\left(\mu r\frac{\partial u_{\mathrm{g}}}{\partial r}\right)-\frac{\Delta P}{\Delta x} \tag{3}$$

Radial momentum

$$\frac{\partial\left(\varepsilon\rho_{\mathrm{g}}u_{\mathrm{g}}v_{\mathrm{g}}\right)}{\partial x}+\frac{1}{r}\frac{\partial\left(\varepsilon\rho_{\mathrm{g}}rv_{\mathrm{g}}v_{\mathrm{g}}\right)}{\partial r}=-\varepsilon\frac{\partial P}{\partial r}+\frac{\partial}{\partial x}\left(\mu\frac{\partial v_{\mathrm{g}}}{\partial x}\right)+\frac{1}{r}\frac{\partial}{\partial r}\left(\mu r\frac{\partial v_{\mathrm{g}}}{\partial r}\right)-\frac{\Delta P}{\Delta r} \tag{4}$$

Gas species equation

$$\frac{\partial}{\partial x}\left(\varepsilon\rho_g Y_k u_g\right)+\frac{1}{r}\frac{\partial}{\partial r}\left(\varepsilon\rho_g Y_k v_g\right)+\frac{\partial}{\partial x}\left(\varepsilon\rho_g D_k\frac{\partial Y_k}{\partial x}\right)+\frac{1}{r}\left(\varepsilon\rho_g rD_k\frac{\partial Y_k}{\partial r}\right)=\varepsilon\dot{\omega}_k W_k \tag{5}$$

where Y_{k}, D_{k}, $\dot{\omega}_{\mathrm{k}}$ and W_{k} represent the mass fraction for species k, diffusion coefficient, chemical reaction rate, and molecular weight of the gas component, respectively. The reaction of NH_3/H_2/air is treated with detailed kinetics [25], which consists of 35 components and 177 elementary reactions. In this study, the hydrogen blending ratio is defined as the ratio of the H_2 volume to NH_3 volume.

Gas energy equation

$$\frac{\partial\left(\varepsilon\rho_{\mathrm{g}}c_{\mathrm{g}}u_{g}T_{\mathrm{g}}\right)}{\partial x}+\frac{1}{r}\frac{\partial\left(\varepsilon\rho_{\mathrm{g}}c_{\mathrm{g}}rv_{g}T_{\mathrm{g}}\right)}{\partial r}+\sum_{\mathrm{k}=1}^{\mathrm{K}}\rho_{\mathrm{g}}\varepsilon Y_{\mathrm{k}}c_{\mathrm{gk}}\left(D_{\mathrm{k}}\frac{\partial Y_{\mathrm{k}}}{\partial x}\right)\frac{\partial T_{\mathrm{g}}}{\partial x}+\sum_{\mathrm{k}=1}^{\mathrm{K}}\rho_{\mathrm{g}}\varepsilon Y_{\mathrm{k}}c_{\mathrm{gk}}\left(D_{\mathrm{k}}\frac{\partial Y_{\mathrm{k}}}{\partial r}\right)\frac{1}{r}\frac{\partial\left(rT_{\mathrm{g}}\right)}{\partial r}=$$
$$\frac{\partial}{\partial x}\left(\lambda_{g}\varepsilon\frac{\partial T_{g}}{\partial x}\right)+\frac{1}{r}\frac{\partial}{\partial r}\left(\lambda_{g}\varepsilon\frac{\partial(rT_{g})}{\partial r}\right)-h_{v}\left(T_{g}-T_{s}\right)-\varepsilon\sum_{k}\dot{\omega}_{k}W_{k}h_{k} \tag{6}$$

where λ_{g}, c_{g} denotes thermal conductivity and specific heat of mixture; T_{s} is the solid temperature. The convective heat transfer coefficient h_{v} is calculated using the following formula [21],

$$h_{\mathrm{v}}=\frac{S_{\mathrm{v}}\lambda_{\mathrm{g}}}{d_{\mathrm{p}}}Nu;Nu=3.7Re^{0.38}Pr^{0.25};Re=\frac{\rho_{\mathrm{g}}ud_{\mathrm{p}}}{\mu_{\mathrm{g}}};Pr=\frac{c_{\mathrm{p}}\mu_{\mathrm{g}}}{\lambda_{\mathrm{g}}} \tag{7}$$

Solid Phase Energy Equation

$$\frac{\partial}{\partial x}\left[\left(\lambda_{\mathrm{eff}}+\lambda_{\mathrm{rad}}\right)\frac{\partial T_{\mathrm{s}}}{\partial x}\right]+\frac{1}{r}\frac{\partial}{\partial r}\left[\left(\lambda_{\mathrm{eff}}+\lambda_{\mathrm{rad}}\right)\frac{\partial\left(rT_{\mathrm{g}}\right)}{\partial r}\right]+h_{\mathrm{v}}\left(T_{\mathrm{g}}-T_{\mathrm{s}}\right)=0 \tag{8}$$

The λ_{eff} [15] and λ_{rad} are the solid thermal conductivity of packing bed and radiative thermal conductivity, respectively,

$$\lambda_{\mathrm{eff}}=1857\left(1-\varepsilon\right)T_{\mathrm{s}}^{-0.5332} \tag{9}$$

$$\lambda_{\mathrm{rad}}=\frac{16\sigma T_{\mathrm{s}}^{3}}{3\alpha_{\mathrm{v}}};\alpha_{\mathrm{v}}=\frac{3\left(1-\varepsilon\right)}{d_{\mathrm{p}}} \tag{10}$$

2.2.1 Boundary conditions

(1) Burner inlet

$$T_{\mathrm{g}}=T_{\mathrm{s}}=T_{0},u_{\mathrm{g}}=u_{\mathrm{g,in}},v_{\mathrm{g}}=0,Y_{\mathrm{NH3}}=Y_{\mathrm{NH3,in}},Y_{\mathrm{H2}}=Y_{\mathrm{H2,in}},Y_{\mathrm{O2}}=Y_{\mathrm{O2,in}} \tag{11}$$

(2) Burner outlet

$$\frac{\partial u_{\mathrm{g}}}{\partial x}=\frac{\partial T_{\mathrm{g}}}{\partial x}=\frac{\partial Y_{\mathrm{K}}}{\partial x}=0 \tag{12}$$

(3) Heat loss to the surrounding through burner wall

$$q_{\mathrm{w}}=h_{0}(T_{\mathrm{w,0}}-T_{0}) \tag{13}$$

where h_0 is the natural convective heat transfer coefficient and set as 20 $Wm^{-2}K^{-1}$, which is typical empirical values of natural convection for commonly used insulation materials; $T_{\mathrm{w,0}}$ is the temperature of the outer surface of the insulation layer; The thermal conductivity coefficient of the insulation wall is assigned as λ_{w}=0.3 $Wm^{-1}K^{-1}$.

(4) Radiation heat loss at burner outlet

$$\left(\lambda_{\mathrm{eff}}+\lambda_{\mathrm{rad}}\right)\frac{dT_{\mathrm{s}}}{dx}=-\varepsilon\sigma\left(T_{\mathrm{s}}^{4}-T_{0}^{4}\right) \tag{14}$$

Symmetric boundary conditions are applied along the axis, while the wall surfaces are assigned no-slip velocity boundary conditions.

2.2.2 Solution method and meshing

The governing equations, along with the specified boundary conditions, are solved using ANSYS Fluent 15.0. A user-defined scalar is employed to resolve the solid-phase energy equation, while the pressure-velocity coupling is handled via the SIMPLE algorithm. Convergence residuals for energy

equation set to 10^{-6}, and while convergence residuals for the remaining equations are set as 10^{-3}. In addition, the average temperature of the mass flow rate at the outlet is monitored. To activate chemical reactions, a high solid temperature of 1800 K is set in the downstream of the burner.

The calculation area is discretized into squares with different sizes, three layers of boundary layer is attached at the inner walls, the refiner grid is applied in the combustion reaction zone to accurately solve the chemical reactions. We evaluate the influence of spatial discretization on the predicted temperature distribution within the domain. The results are presented for four distinct mesh resolutions: 0.25 mm, 0.5 mm, 1 mm, and 2 mm for an equivalence ratio (φ) of 0.6, blending ratio (X_{H2}, $X_{H2}+X_{NH3}=1$) of 0.2 with inlet velocities ($u_{g,in}$) of 0.4 m/s, the gas temperature distribution along the x is shown in Fig. 2. The results indicate that a mesh size of 0.25 mm provides a good balance between computational cost and accuracy, thus 0.25 mm meshes are chosen for this computation.

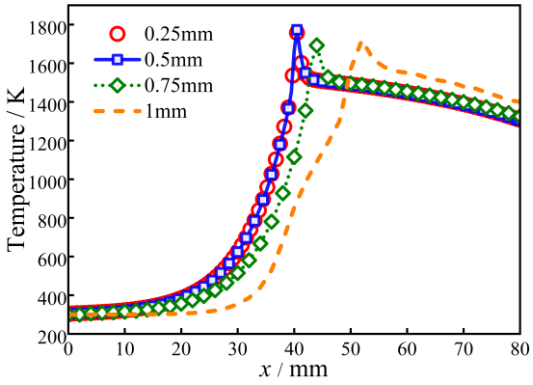

Fig. 2 Grid sensitivity analysis for φ=0.6, X_{H2}=0.2 and $u_{g,in}$= 0.4 m/s

3. Results and discussion

3.1 Influence of inlet velocity on the combustion characteristics

The combustion characteristics of NH_3/H_2/air combustion in porous media are studied under φ=0.6, X_{H2}=0.2 with different $u_{g,in}$. Fig. 3 shows T_g, T_s and enlarged views around the flame zone, the maximum T_g, T_s in the burner, $T_{g,out}$ and net reaction rate of NH_3 along the x. It can be seen from Fig. 3a that stable flames are stabilized just behind the interface of the two sections porous media when $u_{g,in}$ < 0.9 m/s, then the flames are stabilized towards the burner outlet. A continuous increase in the gas temperature before the reaction zone is observed due to the heat recirculating via solid conduction and radiation. Part of the reaction heat is transfer from the reaction zone to the upstream of the burner. The gas is preheated by the solid phase through convective heat transfer between the gas and solid phase. This is a typical characteristic of porous media combustion.

Specifically, for ammonia, which has relatively poor combustion reactivity, effective preheating is achieved before it enters the reaction zone. The addition of hydrogen, of course, also enhances the combustion stability of ammonia. Overall, after blending hydrogen with ammonia, the mixture with an overall equivalence ratio of 0.6 can achieve stable combustion within a flow velocity range of 0.2-0.8 m/s. In contrast, the LFL of pure ammonia in porous media is approximately 0.75 [21]. Therefore, blending hydrogen with ammonia not only extends the LFL but also broadens the range of stable combustion. As shown in Fig. 3b, the gas temperature increases sharply near the flame zone and then decreases along the flow direction, the gas delivers heat to the solid phase.

The maximum gas and solid temperatures in the burner are shown in Fig. 3c. They are increased softly with inlet velocity due to the increasing in the burner power. The net reaction rate of NH_3 is increased continually and the reaction zone is widened with the inlet velocity for the constant φ=0.6, as shown in Fig. 3d. The profiles of reaction rate are basically parabolic-shaped structure. The gas temperature rapidly increases within the range of x=39-42 mm, indicating that this area is a combustion zone. The gas temperature in the reaction zone is significantly higher than the solid temperature, as shown in Fig. 3b. The highest gas temperature is 1770 K, located at x=40.5 mm. Moreover, intense convective heat transfer occurs between gas and solid in this region, causing a significant increase in solid temperature, with the highest solid temperature reaching around 1500 K at x=41 mm.

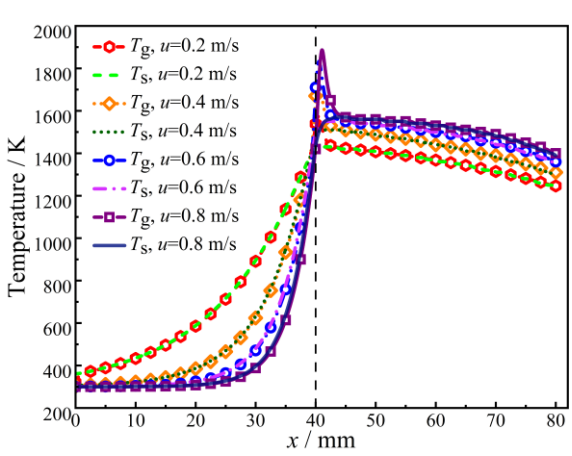

(a) T_g and T_s along the x

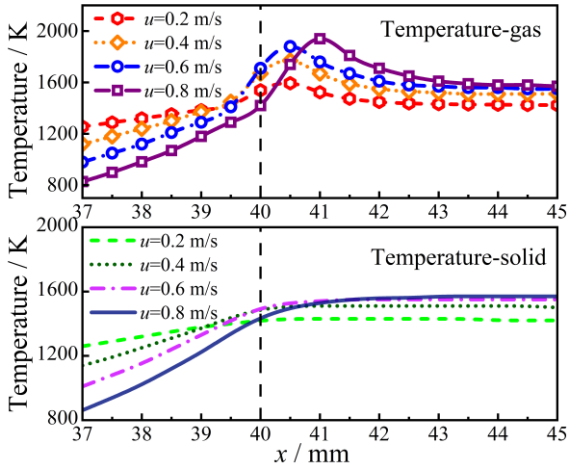

(b) T_g and T_s around the flame zone

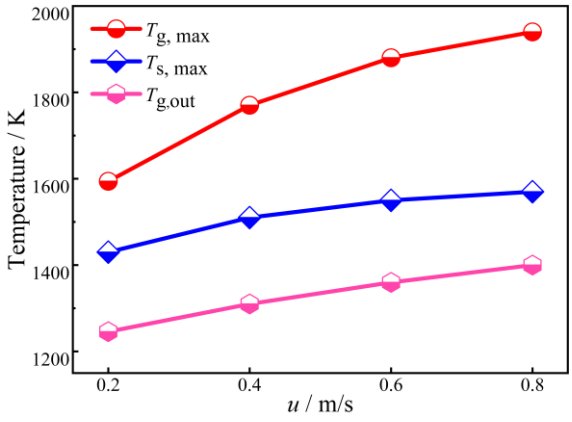

(c) The maximum T_g, T_s in the burner and $T_{g,out}$

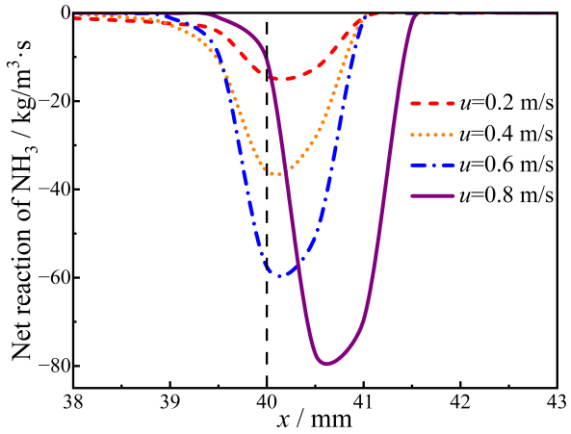

(d) Net reaction rate of NH_3 near the reaction zone

Fig. 3. T_g, T_s and enlarged views around the flame zone, the maximum T_g, T_s in the burner, $T_{g,out}$ and net reaction rate of NH_3 for equivalence ratio of 0.6, blending ratio of 0.2 with different inlet velocities

Fig. 4 illustrates heat of reaction, OH, reaction rate of NO, NO and NO_2 emissions for φ=0.6, X_{H2}=0.2 with different $u_{g,in}$. As shown in Fig. 4a, 4b and 4c, the peak of reaction heat, OH and reaction rate of NO emission are located around the interface for inlet velocity of 0.2 m/s-0.8 m/s and the peaks shifts towards burner outlet when $u_{g,in}$>0.8 m/s. The profiles of these variables are parabolic-shape and its peak values are getting greater with $u_{g,in}$. For example, the maximum reaction heat is increased from

0.0154 W at $u_{g,in}$=0.2 m/s to 0.0789 W at $u_{g,in}$=0.8 m/s.

In combustion systems, OH radicals are commonly used to characterize flame structure and location. As shown in Fig. 4b, the peak OH is increased continually with inlet velocity and the flame thickness is around 2-3 mm, which is significantly greater than that of combustion in open space. The reaction rate of NO reaches its maximum at the flame zone and approaches to zero after the flame zone, as shown in Fig. 4c. This indicates that the NO is mainly formed in the reaction zone.

The Fig. 4d illustrates the emission values of NO and NO_2 as a function of $u_{g,in}$. It is evident from the figure that the emission of NO increases monotonically with $u_{g,in}$, ranging from approximately 5320 ppm at $u_{g,in}$=0.2 m/s to over 18700 ppm at $u_{g,in}$=0.8 m/s. In contrast, the NO_2 emissions, which are scaled by a factor of 50 for better visualization, remain relatively stable across the range of inlet velocities studied, fluctuating around 100 ppm. The N_2O emissions decreased from 2810 ppm to 364 ppm as the inlet velocity $u_{g,in}$ increased. These trends suggest that the inlet velocity has a more pronounced impact on NO formation rather than NO_2 under the given conditions. Such findings are crucial for optimizing the combustion process in porous media to minimize NOx emissions while maintaining efficient energy conversion.

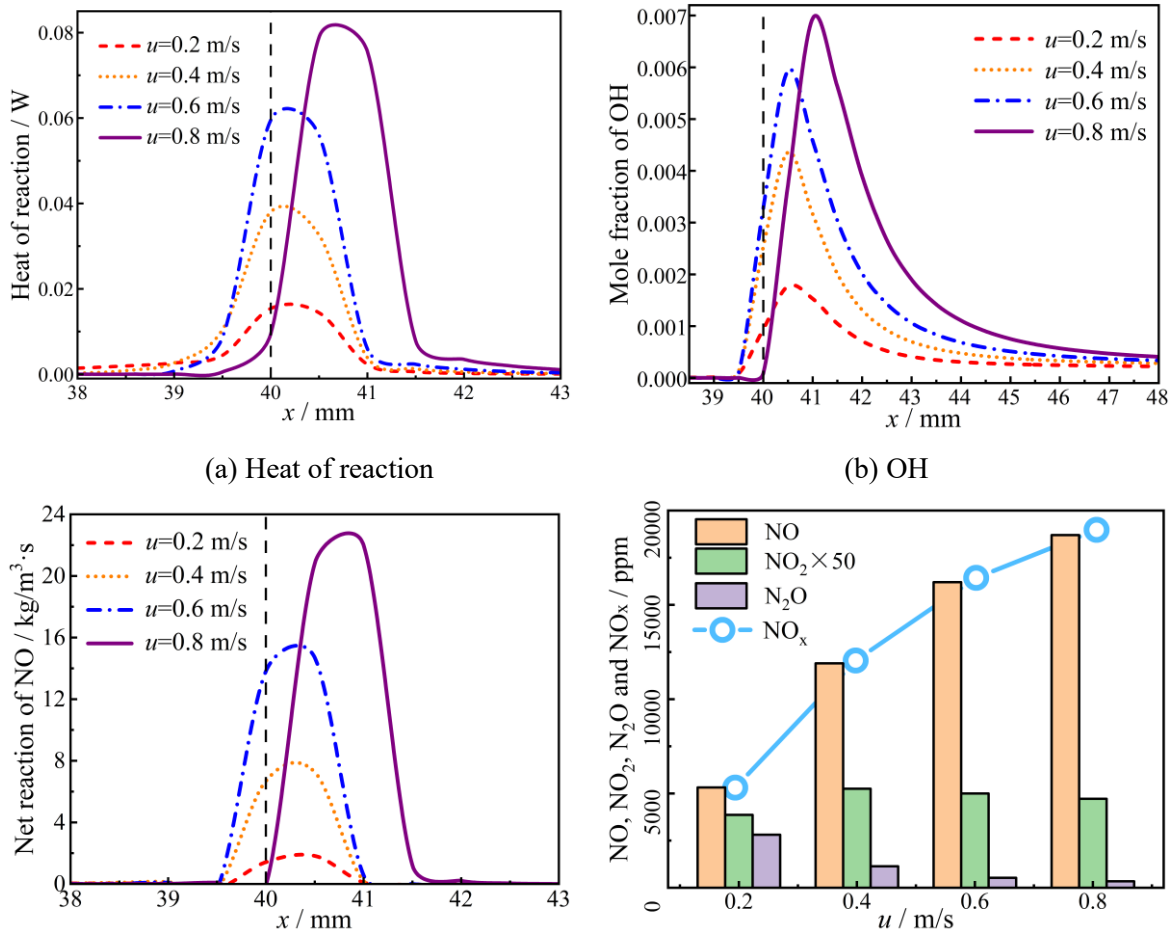

(a) Heat of reaction

(b) OH

(c) Reaction rate of NO

(d) NO, N_2O and NO_2 emissions

Fig. 4 Heat of reaction, OH, reaction rate of NO, NO, N_2O and NO_2 emissions for equivalence ratio of 0.6, blending ratio of 0.2 with different inlet velocities

3.2 Influence of equivalence ratio on the combustion characteristics

The combustion characteristics of NH_3/H_2/air combustion in porous media are further studied under $u_{g,in}$=0.8 m/s, X_{H2}=0.2 with four different φ. As shown in Fig. 5a, the maximum T_g, T_s in the reaction zone and outlet temperature are all increased with φ. For example, the maximum T_g is increased from 1594 K to 1940 K with increasing φ from 0.5 to 0.65. This is because the combustion intensity is increased with φ at the constant $u_{g,in}$=0.8 m/s, X_{H2}=0.2. This is validated by the increasing net reaction rate of NH_3, as shown in Fig. 5b. One can see from the Fig. 5b that the maximum reaction rate is elevated and the flame is stabilized towards the burner inlet along with the enlarged thickness of reaction zone, when φ is increased φ from 0.5 to 0.65. For instance, the maximum reaction rate is increased from 65.8 $kgm^{-3}\cdot s$ at φ=0.5 to 83 $kgm^{-3}\cdot s$ at φ=0.65. Correspondingly, the heat of reaction and the concentration of OH radicals are continuously increased with φ as shown in Fig. 5c and 5d.

Fig. 5c and 5d shows the NO profiles along the x and NOx emission of the porous burner. It is shown in Fig. 5c that the maximum reaction rate of NO is continually increased with φ when φ<0.65 and then the maximum reaction rate of NO is decreased with further increasing in φ. Under the conditions investigated, the production of NO is the dominant NOx formed. The NO concentration exhibits a distinct trend with respect to φ. It initially increases from approximately 14310 ppm at φ=0.5, reaching a peak value of nearly 19690 ppm at φ=0.65. The N_2O emissions decreased from 3760 ppm to 39 ppm as the inlet velocity $u_{g,in}$ increased.

In contrast, NO_2 concentrations are significantly lower than those of NO throughout the entire range of φ examined. These values range from roughly 160 ppm to 68 ppm, visually emphasizing their comparatively minor contribution to the total NOx emissions under these conditions. The total NOx concentration, which is the sum of NO and NO_2, follows a trend similar to that of NO alone due to its dominant contribution. These results indicate that the formation of NO during ammonia combustion is highly sensitive to φ, the NO_2 levels are substantially lower and decrease further as φ moves towards richer conditions.

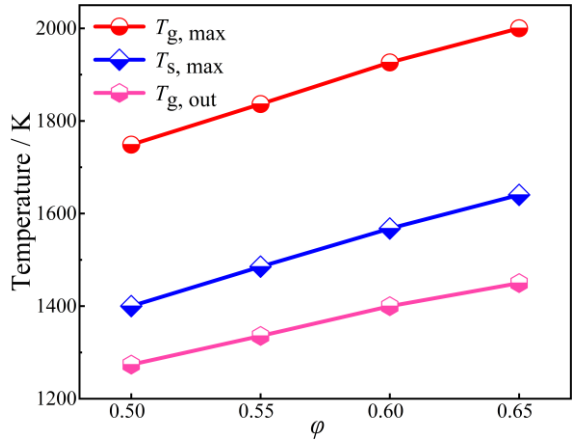

(a) The maximum gas and solid temperature and outlet temperature

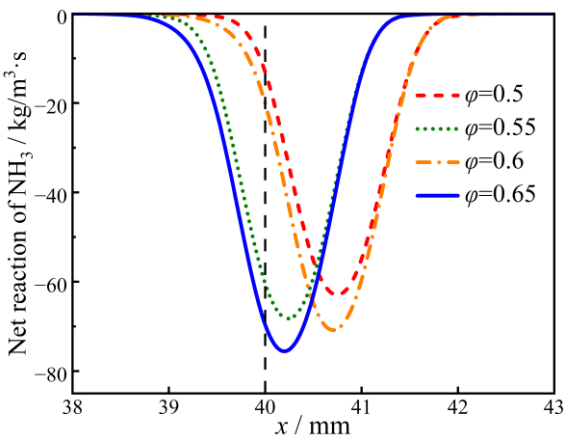

(b) Net reaction rate of NH_3 near the reaction zone

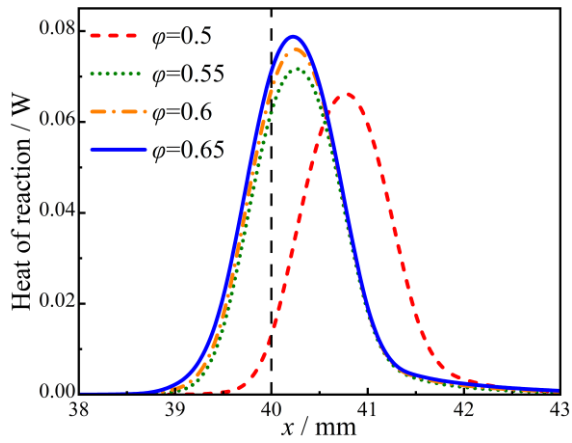

(c) Reaction heat

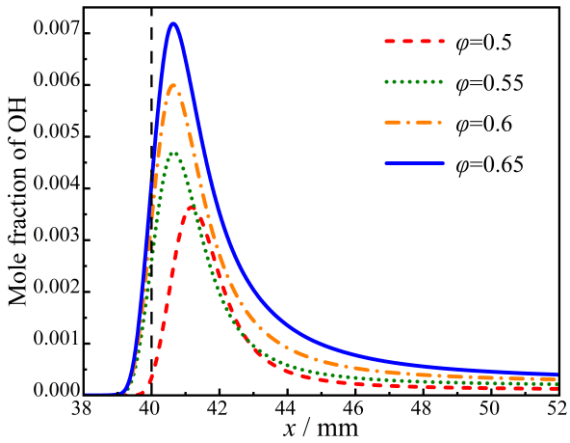

(d) Mole fraction of OH

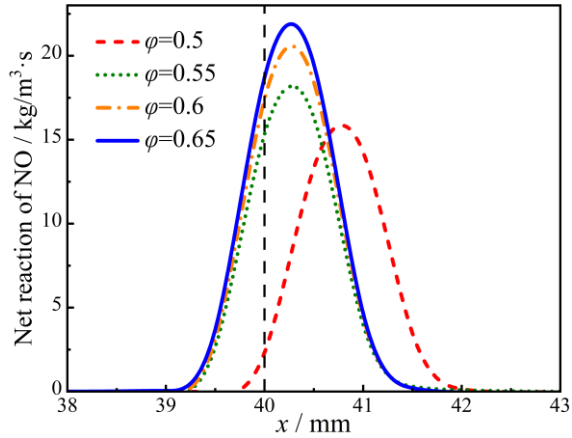

(e) Reaction rate of NO

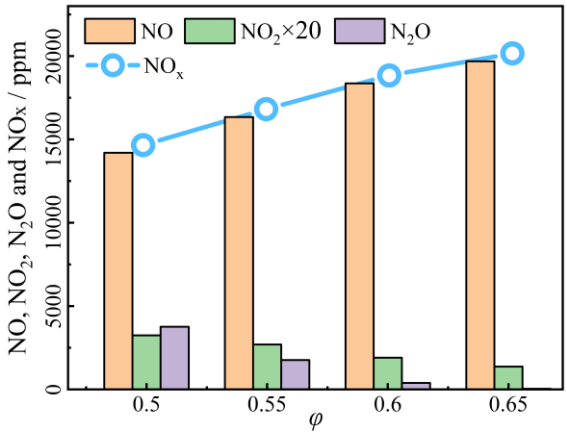

(f) NO, NO_2 ,N_2O and total of NO, N_2O and NO_2 emissions

Fig. 5 The maximum gas and solid temperature, outlet temperature, reaction heat, molar fraction of OH, reaction rate of NO, NO, N_2O, NO_2 along the x-axis and total of NO and NO_2 emissions for blending ratio of 0.2, inlet velocity of 0.8 m/s with different equivalence ratio

3.3. Experimental validation

We have conducted preliminary experimental investigations. The designed combustion experimental system comprises a gas supply system, a burner made of quartz tube, and a measurement system. The burner and porous media, as shown in Figure 6a, have dimensions identical to those used in the numerical simulations. A bare tube is employed to observe the flame, while in other cases, the outer wall of the burner is insulated. NOx concentrations are measured using a Testo 19 instrument, and the flue gas temperature is measured at the burner outlet. This study represents a preliminary investigation; measurements of the temperature inside the porous medium have not yet been performed.

(a)Photo of the burner (b) Flashback (c)Stable combustion (d) Blow out

Fig. 6 The photo of burner, flashback ($u_{g,in}$=0.2m/s, φ=0.8), stable combustion ($u_{g,in}$=0.2m/s, φ=0.6) and blowout ($u_{g,in}$=1.0m/s, φ=0.6)

Figure 7 shows a comparison between the predicted outlet temperatures, NOx emissions and measurements for X_{H2}=0.2, $u_{g,in}$=0.2 m/s with φ= 0.45-0.8. As shown in Fig. 7a, our predictions are generally greater than the experimental values, the maximum relative error is 11.58%, this indicates that our model can capture the variation trend of outlet temperature. However, this needs further cases to validate our numerical model. The NOx emissions by experiments increases softly from 1502 ppm to 2914 ppm as the φ is increased from 0.45 to 0.7, the NOx is decreased to around 2600 ppm with further increase φ to 0.75-0.8. As shown Fig. 7b, the predicted NOx emission are 2 times of the experimental values. At present, precise prediction of NOx is still difficult. As reported by [16], they predicted the same variation trend of NOx emission for NH_3/CH_4/air combustion in porous burner, but the prediction is at least 2 times of the experiment. The predicted NOx emissions for NH_3/H_2/air combustion by the kinetics [19] show good agreement with the experiments, while NOx predicted by the other kinetics [17, 18] are at least 2 times of experiments over wide blending ratio.

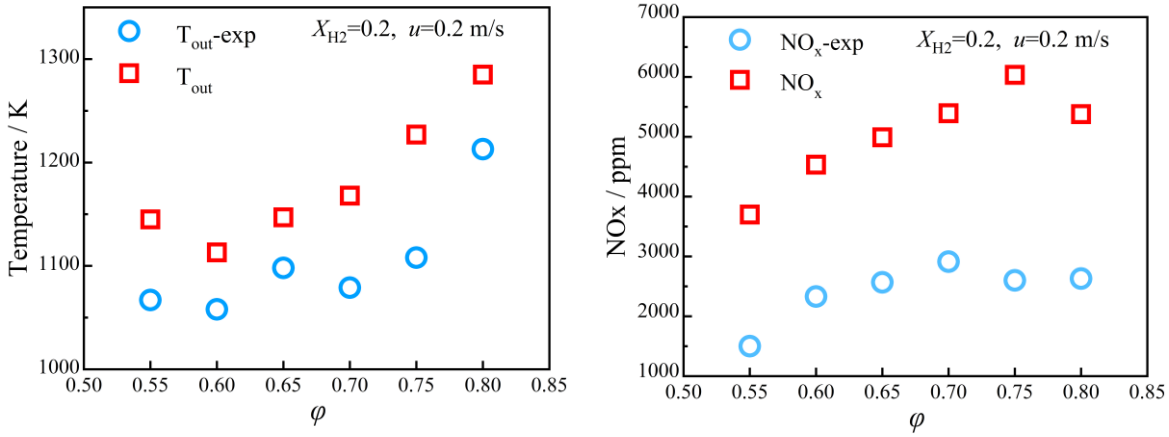

(a) Predicted outlet temperature and measurements

(b) Predicted NOx emissions and measurements

Fig. 7 Predicted outlet temperature, NOx emissions and measurements for blending ratio of 0.2, inlet velocity of 0.2 m/s with equivalence ratio of 0.45-0.8

These deviations could be attributed to several factors, such as the accuracy of the numerical

model in simulating complex chemical reactions and fluid flow behaviors in the porous medium, as well as measurement errors in the experiment. Overall, improvements may be needed to better capture the NOx formation mechanisms at higher equivalence ratios.

4. Conclusion

This study primarily investigates the NH_3/H_2/air combustion characteristics within a two-layer porous burner employing a two-dimensional model with a detailed kinetics. The spatial distributions of gas and solid temperatures, species concentrations, and NOx formation within the porous medium are systematically obtained. Furthermore, the effects of inlet velocity and blending ratio on the combustion are systematically examined. Based on the simulation results, the following key conclusions are drawn:

(1) The gas temperature continuously increases from the inlet before entering the reaction zone due to the heat recirculation via porous medium, thereby expanding the stable combustion limit and lean flammability limit of the NH_3/H_2/air mixture.

(2) Under a hydrogen blending ratio of 20%, the NH_3/H_2 mixed fuel achieves stable combustion in the porous burner when the inlet velocity is within the range of 0.2 m/s to 0.8 m/s and the equivalence ratio is between 0.5 and 0.65. The stable flames are stabilized just behind the interface when $u_{g,in}$<0.9 m/s, then the flames are stabilized towards the burner outlet. The emission of NO increases monotonically with $u_{g,in}$, ranging from approximately 5320 ppm at $u_{g,in}$=0.2 m/s to over 18700 ppm at $u_{g,in}$=0.8 m/s. In contrast, the NO_2 emissions remain relatively stable across the range of inlet velocities studied, fluctuating around 100 ppm.

(3) The flame tends to be stabilized towards the upstream as the equivalence ratio is increasing equivalence ratio from 0.5 to 0.65 under the constant inlet velocity of 0.8 m/s and blending ratio of 0.2, while the NO is increasing linearly from 14310 ppm to 19690 ppm with the equivalence ratio.

(4) A preliminary experimental validation is conducted with the same dimension of the burner and porous media, the same variation trend with the experiment is obtained, but the deviations between the experiments and predictions is obvious.

Although this study has conducted a numerical investigation into the combustion of ammonia blended with hydrogen under varying flow velocities and equivalence ratios, there are certain limitations. Specifically, further exploration is needed regarding the sensitivity of the chemical kinetic mechanism in predicting NOx emissions. Additionally, the inherent limitations of the volume-averaged method may lead to an overestimation of the predicted temperature field.

Acknowledgement

The authors are grateful to the Natural Science Foundation of Shandong Province (ZR2024ME122), Science and Technology Planning Project of Guangdong Province (No. 2024A0505040019) and Guangdong Basic and Applied Basic Research Foundation (No. 2023B1515120012).

Nomenclature

c_g – specific heat, [$kJkg^{-1}K^{-1}$]

d_p –average pore size, [mm]

D_k –diffusion coefficient of species k, [cm^2s^{-1}]

h_k – the molar enthalpy of species [$kJkg^{-1}$]

h_0 – natural convective coefficient, [$Wm^{-3}K^{-1}$]
h_v – convective coefficient, [$Wm^{-3}K^{-1}$]
P – pressure, [Pa]
r – radial coordinate, [m]
T – temperature, [K]
T_0 – ambient temperature, [K]
u_g – axial velocity, [ms^{-1}]
v_g – radial velocity, [ms^{-1}]
W_i – molecular weight of species i, [$kgkmol^{-1}$]
x – axial coordinate, [m]
Y – mass fraction, [-]

Greek symbols

ε – porosity, [-]
λ – thermal conductivity, [$Wm^{-1}K^{-1}$]
λ_{eff} –effective thermal conductivity of packed bed, [$Wm^{-1}K^{-1}$]
λ_s –thermal conductivity of packing bed, [$Wm^{-1}K^{-1}$]
μ – dynamic viscosity, [Pas]
ρ – density, [kgm^{-3}]
σ –Stephan-Boltzmann constant, [$Wm^{-2}K^{-4}$]
φ – equivalence ratio
$\dot{\omega}_k$ – reaction rate of species k, [$Kmol/m^3 \cdot s$]

Subscripts

g – gas
s – solid

References

[1] Kang, L. W., *et al*., A review on ammonia blends combustion for industrial applications, *Fuel, 332* (2023), 126150.

[2] Lan R., *et al*., Ammonia and related chemicals as potential indirect hydrogen storage materials, *Hydrogen Energy, 37* (2012), 2, pp. 1482-1494.

[3] Elishav, O., *et al*., Progress and prospective of nitrogen-based alternative fuels, *Chemical Review, 120* (2020), 12, pp. 5352-5436.

[4] Wang, J., *et al*., Exploring reaction mechanism for ammonia/methane combustion via reactive molecular dynamics simulations, *Fuel, 331* (2023), 125806.

[5] Wang, B. B., *et al*., Effect of diesel-ignited ammonia/hydrogen mixture fuel combustion on engine combustion and emission performance, *Fuel, 331* (2023), 125865.

[6] Makaryan, A. I., *et al*., Combustion of ammonia-blended fuels in porous media burners, with storage and distribution implications: A review, *Renewable and Sustainable Energy Reviews, 220* (2025), 115884.

[7] Hong, Y., *et al*., Atomic insights into the NH_3/CH_4 combustion in air assisted by an electric field, *International Journal of Hydrogen Energy, 135* (2025), pp. 257-266.

[8] Sun, M., *et al*., Flow and heat transfer characteristics of anisotropic Kelvin cells: Influence of stretching ratio and mechanistic analysis, *International Communications in Heat and Mass Transfer, 169* (2025), 109896.

[9] Li, K., *et al*., Steam reforming mechanism of methane using thermodynamics and molecular dynamics, *Journal of the Energy Institute, 121* (2025), 102181.

[10] Shi, J. R., *et al*., Self-sustained stable combustion of off-gas from Solid Oxide Fuel Cell in a cone-shaped porous burner with preheaters, *Energy, 312* (2024), 133566.

[11] Chen, X. J., *et al*., Experimental and numerical investigation on the performance of meso-scale

burners with novel ordered porous media, *Applied Thermal Engineering, 233* (2023), 121103.

[12] Sobhani, S., *et al*., Experimental feasibility of tailored porous media burners enabled via additive manufacturing, *Proceedings of the Combustion Institute, 38* (2020), pp. 6713-6722.

[13] Ellzey, J. L., *et al*., Heat recirculating reactors: fundamental research and applications, *Proceedings of the Combustion Institute, 72* (2019), pp. 32-58.

[14] Nozari, H., et al., Porous medium based burner for efficient and clean combustion of ammonia-hydrogen-air systems, *International Journal of Hydrogen Energy, 42* (2017), 21, pp. 14775-14785.

[15] Lv, J. S., *et al*., Effect of preheating on extending lean extinction limit of ammonia/air combustion in a two-section porous burner, *Journal of the Energy Institute, 116* (2024), 101708.

[16] Rocha, R. C., *et al*., Combustion of NH_3/CH_4/air and NH_3/H_2/air mixtures in a porous burner: experiments and kinetic modeling, *Energy and Fuels, 33* (2019), 12, pp. 12767-12780.

[17] Tian, Z., *et al*., An experimental and kinetic modeling study of premixed $NH_3/CH_4/O_2$/Air flames at low pressure, *Combustion and Flame, 156* (2009), 7, pp. 1413−1426.

[18] Okafor, E. C., *et al*., Experimental and numerical study of the laminar burning velocity of CH_4-NH_3-air premixed flames, *Combustion and Flame, 187* (2018), pp. 185−198.

[19] Chemical-Kinetic Mechanisms for Combustion Applications, Mechanical and Aerospace Engineering (Combustion Research), University of California, San Diego, http://combustion.ucsd.edu.

[20] Vignat, G., *et al*., Combustion of lean ammonia-hydrogen fuel blends in a porous media burner, *Proceedings of the Combustion Institute, 39* (2023), 4, pp. 4195-4204.

[21] Vignat, G., *et al*., Experimental and numerical investigation of flame stabilization and pollutant formation in matrix stabilized ammonia-hydrogen combustion, *Combustion and Flame, 250* (2023), 112642.

[22] Chen, D. N., *et al*., Study on combustion characteristics of hydrogen addition on ammonia flame at a porous burner, *Energy, 263* (2023), 125263.

[23] Jiang, L. S., *et al*., Evaluation of stability enhancement and CO reduction in wake reactor at fine combustion states: PIV measurements and POD flame structure analysis, *Chemical Engineering Journal, 505* (2025), 159633.

[24] Jiang, L. S., *et al*., Visualization on the turbulent structure and restructure characteristic in the wake of a packed bed reactor: PIV measurements and POD analysis, *Renewable Energy, 246* (2025), 122895.

[25] Han, X. L., *et al*., Experimental and kinetic modeling study of laminar burning velocities of NH_3/air, NH_3/H_2/air, NH_3/CO/air and NH_3/CH_4/air premixed flames, *Combustion and Flame, 206* (2019), pp. 214-226.

Received: 17.11.2025.
Revised: 16.01.2026.
Accepted: 15.04.2026.